ADAPTIVE MULTIGRID DOMAIN DECOMPOSITION SOLUTIONS FOR VISCOUS INTERACTING FLOWS

Stanley G. Rubin and Kumar Srinivasan
Department of Aerospace Engineering and Engineering Mechanics
University of Cincinnati
Cincinnati, Ohio

Abstract

Several viscous incompressible flows ,with strong pressure interaction and/or axial flow reversal are considered with an adaptive multigrid domain decomposition procedure. Specific examples include the triple deck structure surrounding the trailing edge of a flat plate, the flow recirculation in a trough geometry, and the flow in a rearward facing step channel. For the latter case, there are multiple recirculation zones, of different character, for laminar and turbulent flow conditions. A pressure-based form of flux-vector splitting is applied to the Navier-Stokes equations, which are represented by an implicit lowest-order reduced Navier-Stokes (RNS) system and a purely diffusive, higher-order, deferred-corrector. A trapezoidal or box-like form of discretization insures that all mass conservation properties are satisfied at interfacial and outflow boundaries, even for this primitive-variable non-staggered grid computation.

Introduction

Viscous interactions are typically associated with turbulent or high Reynolds number (Re) laminar flows. These interactions are quite frequently characterized by the appearance of high flow gradients that are most significant in small or 'thin' domains of finite extent, and in one or more directions, e.g., boundary or vortical layers/regions, triple deck structures, shock wave structure. Outside of these regions, the flow is generally more highly diffused or inviscid so that the flow gradients are less severe. However, the flow character in these smoother regions, which generally encompass a major portion of the flow domain, can be significantly influenced by the interaction with the high gradient layers. In order to accurately assess this class of viscous interacting flows with discrete computational methods, (1) local grid refinement is required in the high shear layers, and (2) simple, efficient, adaptive methods, that effectively communicate information between the disparate flow domains, and at the same time maintain all conservation properties, are necessary.

In the present investigation, an adaptive, multigrid, domain decomposition strategy is combined with a pressure-based form of flux vector discretization in order to accomplish these goals[1-4]. The governing Navier-Stokes equations are evaluated through an implicit, lowest-order in Re, reduced Navier-Stokes (RNS) subsystem[1,2], that is combined, when necessary, with an explicit purely diffusive deferred-corrector (DC) in viscous layers. Local directional refinement that is driven by specified flow parameters and accuracy limits is achieved by sequentially splitting the overall flow domain into a variety of subdomains. In the present analysis, this domain decomposition strategy is applied, in conjunction with an adaptive multigrid algorithm, in order to achieve the appropriate level of grid refinement. In this approach, each grid in the multigrid hierarchy, is of equal or lesser extent than all of the coarser predecessors. The subgrids are split into several multidimensional subdomains that are defined by specified directional and global resolution requirements. A similar approach has been presented for cavity and backstep geometries in a recent publication[5]; although, no attempt was made to meet the differing needs for refinement in two or more coordinate directions. In the present investigation[6-8], this is achieved with a subdomain procedure that allows for segmentally varying grid resolution in two or more directions throughout the flow field. This leads to more optimal grid refinement, and, through the adaptive multigrid procedure, information is very effectively transferred between high and low gradient domains that have distinctly different grid structure. In addition, the equation solver can differ from subdomain to subdomain, e.g., direct solvers can be used in strong interaction domains, line relaxation in moderate interaction domains, etc.

In the present analysis, several two-dimensional, steady, incompressible, large Re laminar and turbulent flow examples are reviewed and the results are compared with other computations or experiments. The problems to be discussed include, the laminar trailing edge (triple deck) flow past a finite flat plate, the laminar recirculating flow associated with a trough geometry, and the laminar and turbulent flows in a backstep channel. The use of pressure-based flux splitting and a trapezoidal or box-like discretization for the implicit RNS subsystem leads to a precise prescription of the surface normal boundary conditions on the local subdomain boundaries. This ensures that interfacial and global mass conservation requirements are automatically satisfied. This is generally not the case with some characteristic-based Navier-Stokes schemes, where special conditions are required in order to satisfy interfacial and global mass conservation. The primitive variable system considered herein is also directly applicable on non-staggered grids. This differs from many other incompressible primitive variable Navier-Stokes formulations, that require pressure Poisson solver or artificial compressibility concepts.

Governing Equations and Discretization

The governing Navier-Stokes equations, shown here in sheared cartesian coordinates, is written for incompressible flow in non-conservation form:

$$u_\xi + v_\eta = 0 \qquad \text{Continuity. (1a)}$$

$$uu_\xi + uy_b'(V+y_b'u)_\xi + V[(1+y_b'^2)u_\eta + y_b'v_\eta] + p_\xi = \frac{1}{Re}u_{\eta\eta} + DC \qquad \xi\text{-momentum. (1b)}$$

$$u(V+y_b'u)_\xi + V(V+y_b'u)_\eta + p_\eta = DC \qquad \eta\text{-momentum. (1c)}$$

where $\xi = x$; $\eta = y - y_b(x)$; $V = v - y_b'u$ is the contravariant velocity component in the η or normal direction (for $y_b'(x) << 1$) ; $y_b(x)$ is the surface definition and (u,v) are the cartesian velocities in the (x,y) directions.

For turbulent computations, the k-ϵ model is employed. This introduces two additional equations for k and ϵ. These equations in cartesian coordinates and non-dimensional form are given as:

$$\bar{u}\frac{\partial k}{\partial x} + \bar{v}\frac{\partial k}{\partial y} = 2C_\mu\frac{K^2}{\epsilon}\left[\left(\frac{\partial \bar{u}}{\partial x}\right)^2 + \left(\frac{\partial \bar{v}}{\partial y}\right)^2 + \frac{1}{2}\left(\frac{\partial \bar{u}}{\partial y} + \frac{\partial \bar{v}}{\partial x}\right)^2\right] - \epsilon + \frac{1}{R_e}\frac{\partial}{\partial y}\left[\left(1 + \frac{\nu_t}{\sigma_k}\right)\frac{\partial k}{\partial y}\right]$$

$$\bar{u}\frac{\partial \epsilon}{\partial x} + \bar{v}\frac{\partial \epsilon}{\partial y} = 2C_\mu C_{\epsilon 1} k\left[\left(\frac{\partial \bar{u}}{\partial x}\right)^2 + \left(\frac{\partial \bar{v}}{\partial y}\right)^2 + \frac{1}{2}\left(\frac{\partial \bar{u}}{\partial y} + \frac{\partial \bar{v}}{\partial x}\right)^2\right] - C_{\epsilon 2}\frac{\epsilon^2}{k} + \frac{1}{R_e}\frac{\partial}{\partial y}\left[\left(1 + \frac{\nu_t}{\sigma_\epsilon}\right)\frac{\partial \epsilon}{\partial y}\right]$$

where $\nu_t = \dfrac{C_\mu k^2 R_e}{\epsilon}$ and C_μ, $C_{\epsilon 1}$, $C_{\epsilon 2}$, σ_e and σ_k are predetermined dimensionless constants which have the values 0.09, 1.44, 1.92, 1.0 and 1.3 respectively. A modified k-ϵ model was recommended by Thangam [17] in which the value of the constant $C_{\epsilon 2}$ is changed from 1.92 to 11/6. This was shown to give much better results for the backstep channel geometry.

A three layer law of the wall is used at the upper and lower walls. This is given as:

$$u^+ = \begin{cases} y^+ & \text{for } y^+ \le 5 \\ -3.05 + 5\ln y^+ & \text{for } 5 < y^+ \le 30 \\ 5.5 + 2.5\ln y^+ & \text{for } y^+ > 30 \end{cases}$$

where $y^+ = yu_\tau/\nu$ and $u^+ = \bar{u}/u_\tau$.

The RNS approximation is given by the lowest-order system obtained by omitting the purely diffusive deferred-corrector (DC) terms. These terms are retained selectively in some subdomains, when they are important. The RNS system is in effect a composite of the Euler and 2nd order boundary layer equations[1-3]. Trapezoidal or 'box' two point $(i,j\pm 1/2)$ differencing is used for all normal derivatives in the first-order (in η) RNS equations (1a,1c), and three point central (i,j) differencing (in η) is applied for the axial momentum equation (1b). If a shear factor $\sigma = \mu u_y$ is introduced in (1b), a box-scheme can in fact be developed for the entire RNS system (1). All axial (ξ) convective and pressure derivatives are upwind differenced with a pressure-based form of flux vector splitting[3], wherein the p_ξ term is represented, for compressible flow, by

$$p_\xi = \omega_{i-1/2}(p_i - p_{i-1})/\Delta\xi_i + (1-\omega_{i+1/2})(p_{i+1} - p_i)/\Delta\xi_i,$$

and $\omega_{i\pm 1/2} = [\gamma M_\xi^2/(1 + (\gamma-1)M_\xi^2), 1]_{min}$.

Here, M_ξ is the streamwise Mach number and γ is the ratio of specific heats. This reduces to a simple 'forward' difference for incompressible flow, so that the elliptic acoustic interaction or upstream influence is introduced through the $p_\xi = (p_{i+1} - p_i)/(\Delta\xi)_i$ contribution. For reverse flow regions, additional negative eigenvalues or upstream influences appear through the convective terms.

A simple line relaxation procedure is used to solve the system of equations for k and e. The differencing used for the k,e equation is consistent with the pressure flux-split discretization. The law of the wall provides the boundary conditions one point away from either wall, which can then be used to implicitly to solve for k and e at any given station. The k-e equations are decoupled from the governing RNS equations. Each pressure relaxation sweep is followed by a sweep to solve the k,e equations using the latest available values for $\bar{u}$, $\bar{v}$. This procedure is convergent.

Grid Structure

In general, the N^{th} multigrid level consists of several subdomains. Each multigrid level has an equal or lesser extent than the coarser grids of the multigrid hierarchy. The first two grid levels cover the entire computational domain. The mesh size is initially quite coarse in the directions in which adaptivity is to be prescribed. Each of the multigrid levels comprise several subdomains, which derive part of their topology from the subdomaining pattern of the coarser predecessor. Within each subdomain, of a given multigrid level the refinement is specified independently. Thus, each subdomain of a multigrid level can act as a parent for a subdomain or subdomains at the next finer multigrid level. If at a given multigrid level, a particular subdomain is refined in only one direction, e.g., η, then on subsequent multigrid levels, further refinement within this subdomain is performed only in the η-direction. A similar strategy is adopted for the ξ-direction. Only subdomains that result from refinement of a parent subdomain in both the ξ and η directions require further decomposition according to the direction selective refinement specifications.

Refinement Strategy

In most adaptive gridding methods, on any grid level, an estimate of the truncation error of the discretized system of equations is used to identify those regions that require finer grid resolution[5]. The overall truncation error estimates, however, do not provide information on the specific direction(s) that require refinement. Therefore for regions requiring higher resolution, the grid is refined in both directions, even though only one coordinate gradient may be significant. In order to achieve directional refinement adaptivity it is necessary to monitor the truncation error of selected gradients or derivatives. For the problems considered herein, the truncation error for the pressure and vorticity gradients, e.g., p_ξ and $u_{\eta\eta}$, are monitored in order to define the regions that require refinement in, ξ and η, respectively. Additional gradient parameters can be added when necessary.

The truncation error estimate is obtained from the solution on two successive grids of the multigrid hierachy. In order to determine the truncation error in a ξ (and/or

η) derivative, the finer of the two grids must have regions that are refined in the ξ (and/or η) direction(s). Although the p_ξ and $u_{\eta\eta}$ terms are the key derivatives for the present analysis, the truncation error of these terms alone will not suffice to ensure that uniform accuracy is achieved throughout the flow domain. The global truncation error for the full discrete system of equations is monitored for this purpose.

Two types of adaptive calculations are performed for the geometries considered herein.

a. One-dimensional adaptive calculation (semi-coarsening multigrid), with adaptivity in the ξ direction and with a preset stretched η grid.
b. Two-dimensional adaptive calculation, in which the refinement is automated in both directions and uniform grids are used in each subdomain. Grid stretching is not applied, except as the grids change discretely from subdomain to subdomain.

The underlying procedure is identical for both methods. The solution is first obtained on a coarse grid, for those direction(s) in which adaptive multigrid refinement is to be considered. For the semi-coarsening adaptive calculation, refinement is performed only in the ξ direction. The grid is refined over the entire domain, and an improved solution is obtained. From the two full grid solutions, the truncation error of the key derivatives and also of the global discrete system is estimated using Richardson extrapolation. Two types of refinement criteria are used. In one procedure, a tolerance is set for the raw truncation error and, in the other, a tolerance is set for a truncation error normalized with the maximum value. The results obtained with the two methods, i.e., identification of the regions that require refinement in the respective direction(s) are quite similar.

For the one-dimensional (in ξ) adaptive calculation only one subdomain results. This decreases in extent as the grid level increases. For the problems considered herein, the significant flow gradients in ξ are centered around the small region $|\xi| < \xi_0$. For more complicated flows, it is possible that disjoint subdomains in ξ will result. For the two dimensional adaptive calculation, however, the various regions will have different refinement requirements; therefore, it is necessary to define regions that have disparate grid requirements. Subdomains requiring refinement in the η direction, or the ξ direction, or in both (ξ,η) directions, are identified. Although different meshes are used in different regions, within each subdomain, a uniform grid is specified. This procedure is applied on the third and higher levels of the multigrid hierarchy. The calculation proceeds with intergrid multigrid transfers. On convergence, the truncation error estimation process is repeated with the N^{th} multigrid and the stored $(N-1)^{th}$ multigrid level grid solutions.

Multigrid Implementation

For the RNS system of equations (1), without DC, a semicoarsening multigrid procedure has been presented previously[9,10] to accelerate the convergence of the global pressure relaxation procedure[1,2]. A von Neumann analysis of the linearized form of the RNS system shows that the rate of convergence of the global procedure is dictated by the maximum eigenvalue λ, as given by

$$\lambda = 1 - c_1 \pi^2 (\Delta\xi)^4 N_\xi^2 / \eta_M^4,$$

where c_1 is a constant of 0(1); N_ξ is the number of stations in the ξ direction; η_M is the normal boundary location, and $\Delta\xi$ is the axial step size. The convergence rate is significantly improved if the extent of the domain in the two directions is reduced. *The current multigrid domain decomposition procedure, in effect, reduces η_M whenever a fine $\Delta\xi$ is specified, and thereby achieves comparable 'coarse grid' convergence rates on fine grids.*

In the present application the multigrid method is implemented in a Full Approximation Storage (FAS) mode. The global pressure relaxation procedure considered herein essentially reduces to a block SOR procedure (in ξ) for the pressure in attached flows and for the pressure and velocities in reversed flow regions. At each station, an implicit, fully coupled tridiagonal system is inverted. When highly stretched grids are used in η to resolve the boundary layer, the semi-coarsening mode of the multigrid method has been shown to be more effective than the standard full coarsening mode. In this mode, the streamwise grid alone is coarsened when the calculation shifts to coarser grids. The same η grid is retained throughout. Significant gains in the overall effort have been achieved with this approach[9,10].

A source term (IST), first introduced by Israeli[11], is required in order to achieve satisfactory performance of the multigrid procedure[10]. The IST acts as a form of under-relaxation or smoother for the pressure field. This leads to much smoother residual fields, which are essential for good representation on the coarser grids. However the IST leads to a slower asymptotic convergence rate on any given grid. The domain decomposition procedure reduces this limitation to a large extent. Since the truncation error in the p_ξ term is used to determine regions needing refinement in the ξ direction, subdomains in which the grid is only refined in the η direction, will generally have a reasonably converged pressure field from the coarser grid. Thus it is possible to perform the multigrid calculation without the IST smoother in these subdomains.

In the present investigation, the one-dimensional adaptive calculation adds an element of sub-domaining to the semi-coarsening analysis[9,10], so that only portions of the global domain require fine grid resolution in the ξ direction. For the two-dimensional adaptive calculation, the multigrid algorithm is implemented in the standard full coarsening for domains that require refinement in both directions and the semi-coarsening mode for those domains requiring refinement in only one direction. One fine grid work-unit is comprised of one sweep in each subdomain belonging to a given multigrid level. This also includes the interdomain transfer processes. The decision to move the calculation back to a coarser grid is based on the rate of convergence on each subdomain. If the ratio of the residual norm between two successive global iterations, in any subdomain belonging to that multigrid level, falls below a certain value, typically 0.85-0.95, then the calculation is restricted to the coarser level. The fine grid solution is not

corrected until the residuals in the coarse grid subdomains are all reduced to a value one order-of-magnitude lower than the maximum residual over all subdomains in the finer level. The multigrid components are summarized as follows,

a. Relaxation: $u_n^k = S^k u_{n-1}^k$, where S^k is the global pressure relaxation operator and u^k on convergence satisfies $L^k u^k = f^k$. Here k represents the present or finest multigrid level and n represents the iterate. $L^k u^k = f^k$ is the discrete approximation of the continuous problem $Lu = f$

b. Restriction to coarse grid where the following equations are solved: $L^{k-1}u^{k-1} = I_k^{k-1} r_n^k + L^{k-1}\hat{I}_k^{k-1} u_n^k$ for points on the coarse grid which lie within the fine grid and $L^{k-1}u^{k-1} = f^{k-1}$ for points on the coarse grid that lie outside the extent of the fine grid. Here $r_n^k = f^k - L^k u_n^k$. I_k^{k-1} and $\hat{I}_k^{k-1}$ are fine to coarse grid transfer operators. The full-weighting operator recommended by Brandt[12] is used to transfer the residuals and the solution was restricted by using a simple injection operator.

c. Prolongation or correction where the fine grid solution is corrected with the solution from the coarse grid modified problem.
$u_{n+1}^k = u_n^k + I_{k-1}^k (u^{k-1} - I_k^{k-1} u_n^k)$, where I_{k-1}^k is a coarse to fine interpolation operator

It should be noted that in the present calculation, the multigrid transfer operations play a dual role. In addition to accelerating the convergence of the relaxation procedure, they also transmit information from the finer grids to the coarser grids, and thus improve the accuracy of the solution in regions of the coarser grids where refinement was not required. The second term in the multigrid restriction process, acts as a truncation error injection term and improves the discrete approximation on the coarse grid. Thus on the coarser grids, instead of solving $L^{k-1}u^{k-1} = f^{k-1}$ everywhere, we solve $L^{k-1}\hat{u} = \tau$ in part of the domain, where $\tau = L^{k-1}\hat{I}_k^{k-1} u^k$. This is closer to the continuous problem $Lu = f$. Here L is the continuous counterpart of the discrete operator L^{k-1} and u is the exact solution for the continuous problem; u^{k-1} is the exact solution to the discrete problem and $\hat{u}$ is the improved solution due to the modified right hand side of the discrete approximation.

The deferred-corrector in (1) is input as a prescribed functional form on the right hand side of the fine grid equation. On any given grid level, the calculation is initially considered without the DC term. After a reasonable level of convergence is achieved, e.g., 10^{-3}, the DC term is evaluated from this known solution. This value is prescribed on the finest grid and added explicitly to the right hand side of the equations. This term is transferred to the coarser grid levels through the standard multigrid procedure. If the DC term is introduced earlier, divergence results. This is due to the fact that the solution is initially quite poor and therefore the prescribed DC term is significantly in error. This distorts the differential equation and induces an instability in the pressure during the relaxation procedure. If the RNS solution is allowed to converge moderately before introducing the DC term, the overall solution procedure, with the DC addition, exhibits no significant degradation in rate of convergence for the examples considered herein.

For turbulent flow modelling, the eddy viscosity ν_t is calculated only on the finest grid. The fine grid values of ν_t are injected to the corresponding coarse grid points during the restriction step. The ν_t values, at points on the coarse grid, that lie outside of the extent of the fine grid are not updated. This procedure is validated by calculations that do not include any adaptivity. In this case, the fine grid extent is the same as that of the coarse grid. Therefore, the ν_t values at all points on the coarse grid will be updated. The results obtained from this full refinement calculation and those from the fully adaptive multigrid calculations are identical.

Interdomain Transfer of Boundary Conditions and Conservation at Grid Interfaces

For a given subdomain, the following boundary conditions are to be prescribed:

$u = v = 0$ at $\eta = 0$; $u = 1$, $p = 0$ at $\eta = \eta_{max}$; $p_\xi = 0$ or p prescribed at $\xi = \xi_{max}$; u and v are given by freestream values at $\xi = \xi_0$.

For external flows, if a subdomain has its outflow at some $\xi < \xi_{max}$ then the boundary condition on pressure changes from Neumann to Dirichlet type. For internal flow, the outflow boundary condition is Dirichlet type for the pressure. Also, if the lower boundary of a subdomain is at some $\eta > 0$, then non-zero velocities have to be prescribed. In time-dependent, characteristic-based, Navier-Stokes computations, that use locally embedded grids, boundary conditions are required for all variables, i.e., u, v, and p. In addition, special care has to be taken to ensure that mass conservation is not violated locally or globally.

In the pressure-based trapezoidal or 'box' formulation, this difficulty does not occur as the normal velocity v in η, or u in ξ, is not prescribed at the upper or lower, or outflow boundaries. Only the tangential component u is prescribed at the upper interface or interdomain boundary. The pressure-based box-type differencing allows for the calculation of the normal velocity at the outer boundaries and the pressure at the body surfaces. The normal velocity is computed from the continuity equation and therefore mass conservation is automatically satisfied on all levels, for all subdomains. This eliminates the need for special interpolation formulae to ensure conservation of mass when the boundary conditions are prescribed from the coarse grid solution. Thus weak instabilities, that arise when such methods are applied in Navier-Stokes formulations without satisfying mass conservation, do not appear in the present method. Direct evaluation of the pressure at the inflow or lower boundaries with the trapezoidal or box discretization also eliminates the need for special pressure boundary conditions.

The calculation is performed sequentially rather than in parallel in the various subdomains. As such the boundary conditions at the inflow and outflow stations for

each subdomain are updated with the latest available values. The overlap allowed in the subdomaining process follows the following rules.

a. The last station of any subdomain, which is at some $\xi < \xi_{max}$ coincides with the first station of the subdomain to its right, (if one exists), where the pressure is computed.
b. Similarly, the inflow station of any subdomain, which is at some $\xi > 0$ coincides with the last station on the subdomain to its left, (if one exists), where the velocities are computed.
c. If the inflow station or the outflow station of a given subdomain coincides with the physical boundaries of the global flow field then the boundary conditions discussed previously for inflow, outflow, upper and lower boundaries are used for these subdomains.
d. If there are no subdomains to the right, for the cases in a), or if there are no subdomains to the left, for the cases in b), then these boundaries are updated using coarse grid values during the multigrid prolongation process.

In the vertical direction an implicit solver is applied and no overlap is necessary.

If a subdomain has only one of its horizontal boundaries in common with that of another subdomain, then updating the boundary conditions along this edge, after one sweep in all subdomains, leads to iterative divergence on this subdomain. This influence gradually filters through to other subdomains. If these boundaries are updated through the multigrid transfer processes, then the calculation is convergent. This reflects the fact that an update of just one boundary after each sweep, with the other three updated only during the multigrid transfer process, leads to an inconsistency. This constrains the variables from adjusting to changes that occur dynamically, as the solution evolves in the various subdomains. The multigrid transfers provide the correct dynamic response to changes between subdomains.

Results

All of the calculations presented herein are initiated on the coarsest grid, with uniform flow velocity and pressure. On the finer grids, the interpolated coarse grid solution fields are sequentially applied as initial approximations. Since convergence to the final solution is improved with more accurate initial approximations[5,9,10], the adaptive multigrid framework introduces this element in a natural and convenient fashion. It is significant that for all of the examples presented herein, Reynolds number continuation is not required in order to obtain a solution for any of the prescribed values of Re. Even for highly interactive, large Re flows, the solution is obtained directly with uniform initial values at the designated value of Re.

Example 1: Flow over a finite flat plate: the trailing edge problem[6].

Figure 1 depicts the grid obtained for a semi-coarsening (in ξ) adaptive calculation. The η grid is highly stretched and fixed. Note that the finer grids zoom in around the trailing edge, which is located at $\xi = 1.0$ (the figure is scaled by a factor of 2 in the ξ-direction). Significantly, the extent of the finer grids in the η direction is progressively reduced, even when adaptivity is specified only in the ξ direction. Although each multigrid level contains only one subdomain (in ξ) that requires further refinement on subsequent levels, the η extent of this subdomain is affected.

Figure 2 depicts the composite grid obtained with full two-dimensional adaptivity. Within each subdomain, uniform grids, in both the ξ and η directions, are prescribed. Figure 2 is an overlay of seven multigrid levels, each of which comprises several subdomains. In each level, it is found that the subdomain, for which refinement in both directions is required, is centered around the trailing edge. The adaptive computations, both semi-coarsening and two-dimensional, are compared with non-adaptive semi-coarsening multigrid calculations. For the latter, a uniform fine grid in ξ and a highly stretched η grid is prescribed. The grid stretch factor is chosen from the specified minimum and maximum $\Delta\eta$ values, and the location of η_{max} that was applied for the two-dimensional adaptive study. The same η grid is employed for the adaptive semi-coarsening calculation. Figure 3 shows a comparison of the pressure coefficient C_p for the three calculations. There is good agreement in the pressure variation and, in particular, the predicted peak pressures. Table 1 summarizes the computer memory and CPU requirements. These are given as percentages of the non-adaptive, semi-coarsening, calculation. Note that the memory requirement for the one- and two-dimensional adaptive calculations are similar. This signifies that the specified η stretching for the semi-coarsening calculation is reasonable.

Table 1. Summary of Computer Resource Requirements for the finite flat plate calculation

Aspect	Two-D Adaptive	One-D Adaptive	Full Refinement with stretched η grid
CPU	18.03%	15.10%	100.0%
Memory	12.90%	13.22%	100.0%

The adaptive grid of Figure 2 defines the extent of the interaction zone surrounding the trailing edge. From large Re asymptotic triple deck theory, three layers with different length scales have been identified[12], viz., a lower viscous rotational deck of $0(Re^{-5/8})$, a middle inviscid rotational deck of $0(Re^{-4/8})$, and an upper inviscid irrotational deck of $0(Re^{-3/8})$. Since the vorticity is zero in the upper deck, and since vorticity is the monitored parameter for refinement in the η direction, the adaptive procedure should lead to a grid that does not require η refinement in this 'upper deck' region. The grid obtained from the two-dimensional adaptive calculation displays this result quite clearly. At each multigrid level, there is a region away from the body that is in fact refined only in the ξ direction. This region, in the finest multigrid level, represents the extent of the upper inviscid irrotational

region. Estimates for the extent of the other two 'decks' are also obtained from the grid structure. In more complicated flows, e.g., turbulent flow past the same geometry, for which analytical methods cannot be easily developed, the appropriate resolution in each distinct region will be automatically captured with the present multigrid adaptive procedure. In this sense, *the computation results in a form of discrete asymptotic analysis.*

Example 2. Flow over a trough[6].

The second geometry to be considered is the laminar flow over a trough configuration. Both unseparated and reverse flows are computed with the two refinement strategies previously discussed. The trough surface is specified by $y_b = -D\ \mathrm{sech}[4(x-x_0)]$, where D represents the maximum depth, which occurs at the location x_0. The values $x_0=2.5$ and Re = 80000 are used for the present calculation. The grid obtained from the two-dimensional adaptive procedure, for D=0.03 and with a region of flow reversal, is shown in Figure 4. Note that refinement in the η direction extends to a significantly greater distance than was found for the trailing edge geometry. This is due to the fact that the maximum vorticity now occurs near the outer edge of the separation bubble and not at the surface. Also note the sudden increase in the extent of the region where η refinement is performed. This signifies the increase in boundary layer thickness as a result of flow separation. The reversed flow region is essentially vorticity free; however, the current refinement strategy assumes that regions requiring refinement, in the η direction, will always have a lower boundary at the wall. This condition can be modified to allow for multiple η subdomains in the recirculation region. This was not considered necessary for the current calculations. Figure 5 depicts the pressure variations obtained for the three calculations discussed previously for purely attached flow and D=0.015. Figure 6 provides comparisons of the skin friction for the separated (D=0.03) case. Once again good agreement is obtained and significant gains in computer resource requirements are found (Table 2). The locations of the

Table 2. Summary of Computer Resource Requirements for the trough geometry

Aspect	Geometry	Two-D Adaptive	One-D Adaptive	Full MG with non uniform η grid
CPU	Trough (Sep)	18.03%	—	100.0%
	Trough (Unsep)	7.10%	16.80%	100.0%
Memory	Trough (Sep)	16.32%	—	100.0%
	Trough (Unsep)	5.10%	63.4%	100.0%

separation and reattachment points computed by the two-dimensional adaptive calculation are at $\xi=2.31$ and $\xi=2.54$, respectively; the values predicted by non-adaptive full multigrid refinement are at $\xi=2.31$ and $\xi=2.53$. This further confirms the validity of the domain decomposition approach and the advantages of adaptive multigrid over full multigrid. All results presented here are in excellent agreement with all earlier results[1,9] presented for these geometries.

Example 3. Internal flow in a back step channel: laminar[7,8] and turbulent flows.

For this flow, which is dominated by rather large recirculation regions, it is still possible to carry out the calculation for all Re considered herein by prescribing uniform initial flow conditions. This is true even for the relatively difficult, although somewhat artificial two-dimensional calculation with Re=800 (based on channel height). For this Re value, two separation bubbles, one on each wall are evident. Reynolds number continuation, as applied in many other reported NS solvers[14], is still not required for the present calculations. Both laminar (Re=800) and turbulent results are obtained for the back step geometry. The standard two equation k-e model discussed earlier is used for turbulence closure.

For laminar calculation, a step height to channel height ratio of 0.5 is used. The reattachment length (X_R) for the primary recirculation zone is compared in Table 3 for a range of laminar Reynolds numbers. Comparisons are given for the present 2-D adaptive method, full refinement with the standard non-adaptive multigrid method, and earlier calculations by Ferziger[5], Caruso[15] and Sotiropoulos[13]. The calculated reattachment length for the adaptive and non-adaptive procedures is identical to two decimal places; however, the computational effort is considerably less for the former, see Table 4.

Table 3. Comparison of Reattachment Length for Laminar Backstep Channel Flow

Re	Present Calculations		REF [5]	REF [15]	REF [13]
	Adaptive	Non-Adaptive			
133	1.94	1.94	2.0	1.95	1.84
267	3.25	3.25	3.25	3.25	3.17
400	4.32	4.32	4.35	4.40	4.40
600	5.50	5.50	5.35	5.40	5.63

For adaptive refinement in the η direction the truncation error is scanned from the wall towards the outer boundary. For external flow, the vorticity gradient decreases exponentially and a thin layer near the wall, where refinement is maximum, can be identified. This region is specified by fixing the upper boundary at the furthest point, or largest η value taken over all ξ locations, that satisfies the truncation error tolerance. For internal flows, boundary layers, where refinement in η should be required, exist at both boundaries in the normal or η direction. However, the number of grid points that are necessary to resolve the flow gradients in the η direction is

quite moderate and therefore no attempt was made to adaptively refine in this direction. Instead, the full multigrid procedure is applied in the η-direction for each of the subdomains for which ξ-refinement is necessary. This allows for different uniform η grids in the different ξ subdomains.

Table 4. Summary of Computer Resource Requirements for the Backstep Geometry

Aspect	Re	Adaptive Multigrid/Full Refinement NonAdaptive Multigrid
CPU	133	35.49 %
	267	36.15 %
	400	46.23 %
	600	50.40 %
Memory	133	30.80 %
	267	37.44 %
	400	41.49 %
	600	47.49 %

Table 4 displays the computer resource requirements for the backstep channel calculation. For each Reynolds number, the CPU and memory requirements are shown as percentages of the corresponding non-adaptive calculations. Note that as the Reynolds number increases from Re=133 to Re=600, the number of grid points required to resolve the flow field increases. This is expected, as the size of the separation bubble increases with Reynolds number. The number of required grid levels, as well as the finest mesh size for all Reynolds numbers up to Re=600, is identical in each direction. A total of five multigrid levels are defined for all Reynolds numbers up to Re=600. However the subdomain extent for each multigrid level is different for different Re. The extent of the finer grids is governed by the size of the recirculation zone, which increases as Re is increased. For the Re=800 case, six multigrid levels are required, as the change in the solution from level 4 to level 5 is still significant and greater than the specified tolerance.

An increase in computational time and memory requirements is observed as the Reynolds number and associated number of grid points increases. The time required for the full refinement non-adaptive calculation increases only marginally as Re is increased from 133 to 600. This increase is entirely due to the changing nature of the flowfield, since the same grid is used throughout this Re range. More specifically, when the degree of velocity relaxation is increased due to the increasing extent of the reversed flow region, the convergence rate degrades and additional iterations are required to achieve the specified tolerances. Furthermore, the percentage gain in adaptive over non-adaptive procedures is reduced as the Reynolds number increases, e.g., to about 50% at Re=600.

The *effect of location of the outflow boundary* and *the non-reflectivity of the outflow boundary conditions* are important aspects of this study. The adaptive multigrid domain decomposition procedure is initiated on a very coarse grid, and yet, it is possible to place the outflow boundary quite far downstream, e.g., 60 step heights, and still recover very accurate and computer efficient computations. The solutions at the outflow are in almost perfect agreement with the analytic fully developed flow values. Although the finer grids in ξ and η occur in subdomains much further upstream, in and near the reverse flow regions, the influence of the outflow boundary conditions is propagated through the multigrid transfers to and from the coarser grids connecting the various subdomains. This allows for efficient transfer of information without excessive grid specification. In addition, as is shown[8], the RNS pressure flux-splitting procedure allows the outer boundary to be placed very far upstream, e.g., within the upper wall recirculation region, without solution degradation.

For the laminar backstep, the DC terms neglected in the RNS approximation have been included after obtaining a reasonably converged base solution for the RNS system. For this geometry, the vertical wall region near the step corner represents the only portion of the flowfield where the full Navier Stokes terms are of any consequence. Along the vertical wall, the v_{xx} term represents the vortical or diffusive boundary layer influence. It is found[8] that in this region, although the inclusion of the DC term does not produce a significant quantitative difference, some qualitative difference is observed in the solution. Figures 7a-7d depicts the streamwise velocity profile for Re=400 at four successive stations near the corner. Note that the effect of the DC diminishes rapidly away from the corner. A significant difference between the two solutions is associated with a small positive axial velocity that is observed near the corner when the DC is included. This represents a counter rotating vortex within the primary separation bubble. The reattachment length remains unchanged even when the DC is included.

The non-reflectivity of the Dirichlet pressure outflow boundary condition was tested for the severe Re=800 case with calculations on computational domains of three different lengths. It was found that for the cases considered, locating the outflow boundary further upstream did not have a significant effect on any of the solutions. Comparisons of the streamwise velocity profile at the streamwise location X=7 are given in Figure 8. The outflow boundary was located at X=7, X=15 and X=30; the results clearly indicate that the effect of the outflow location on the solutions is minimal. Figure 9 shows the comparison of the stream function contours obtained by placing the outflow at X=7 and X=15. The two contour patterns are identical[8].

A benchmark solution for Re=800 has been published by Gartling[14]. The present solution, which is obtained with the adaptive multigrid domain decomposition procedure, is compared with these results. In Figure 8, comparison with the benchmark solution of the streamwise velocity profiles at X=7 is also shown. Note that reverse flow also occurs on the upperwall. The appearance of this upper separation bubble is thought to introduce three-dimensionality into the flow, and for this reason there is some disagreement between the experimental results and all of the numerical solutions. However, the present results, which are totally grid independent, agree quite well with most of the other numerical computations. Due to the very fine meshes that have been prescribed with the

multigrid domain decomposition procedure, the residuals and truncation errors are quite small and therefore these numerical solutions, are considered to be highly accurate. Figure 10 depicts comparison of vorticity profiles. The agreement with the benchmark contours[14] is excellent throughout. Moreover the results are essentially unchanged with the outflow boundary at X=30 or X=7, which is inside the upper recirculation zone[8] for the Re=800 case.

Figures 11 and 12 show typical grids obtained using the adaptive multigrid procedure for the backstep channel. Figure 11 shows the grid for Re=100 and Figure 12 depicts the grid for Re=267. Note that the region covered by the finest grid is larger in extent for Re=267. This is expected as the region of reversed flow is larger in this case. Note that the grid used in the y-direction is quite coarse far downstream where the flow is fully developed. This reflects the fact that the truncation error is very low in the normal derivatives in this region. Since the fully developed flow profile is parabolic, central differencing will theoretically incur zero truncation error. In streamwise direction, a grid as coarse as $\Delta x=0.5$ can be used towards the outflow without loss of accuracy. The adaptive multigrid procedure clearly utilizes this fact and provides optimal resolution.

The turbulent flow past the backstep channel is of interest in many engineering applications. For the current study, the k-ϵ model has been used to compute the Reynolds stress terms. This model requires that inflow values for k and ϵ be prescribed. For the present calculation these values are generated from a straight channel turbulent flow computation with a step initial profile. The k, ϵ, u and v profiles obtained at the outflow of the straight duct are used as the inflow conditions for the backstep calculation. This inflow is located at a distance five step heights upstream of the step corner. It is noted that the overall nature of the flow field, including the reattachment length is strongly dependent on the inflow values used for k and ϵ. Different profiles for k and ϵ can be generated by varying the length of the straight duct. This will greatly alter the backstep channel solution. A channel length of 23 step height was used to generate the inflow profile for the present calculation. This ensures that the profiles are quite well developed. The corresponding velocities, k and ϵ profiles are then used for the backstep channel calculation. Once again, the inflow is located five step heights upstream of the step corner. Thangam et al.[16] observed that the predicted reattachment length using the standard isotropic k-ϵ model was in error by about 12%, when compared with the experimental value. They showed that a modified k-ϵ model which takes anisotropic effects into account provides improved results. In another study by Thangam[17], it was shown that a modified isotropic k-ϵ model can also lead to improved results. This model, which requires only the variation of a single constant, is considered for some of the calculations presented herein.

The step height to channel height ratio used is 1:3 in the present calculations. A reattachment length (x/H) of 7.04 was obtained for a Re=132000 based on channel height. This is in very good agreement with the experimental value of 7.1. Figure 13 shows the streamfunction contours for the same flow. Note that there is a secondary counter rotating vortex within the primary separation bubble. This was also observed by Thangam et. al[16]. The calculation was also performed by modifying the value of $c_{\epsilon 2}$ to 11/6 as suggested[17]. The reattachment length increased, in this case, to 7.66. This was also the trend observed[17]. Although in their case, the standard k-ϵ model was underpredicting the reattachment length and modifying the constant produced acceptable results.

Summary

An adaptive multigrid domain decomposition method has been used to efficiently compute incompressible laminar and turbulent flows with regions of recirculation and strong pressure interaction. A low order RNS system of equations, a fully consistent primitive variable non-staggered grid solver, accurate mass conservation at subdomain interfaces and global boundaries, non-reflective outflow boundary conditions and a pressure-based flux-split discretization are the key features of the procedure. The adaptive multigrid domain decomposition procedures allows for efficient grid definition consistent with asymptotic theory and for effective transfer of information to and from fine grid high gradient regions to coarse grid 'inviscid' regions.

Significant gains in computer resources have been achieved when compared to standard non-adaptive methods. Good agreement is obtained between the present solutions, standard non-adaptive full refinement computations and other published results. The computational cost is several times smaller than that required by most other NS methods[14]. For example, the CPU required for the backstep channel calculations, with Reynolds numbers in the range 100-600, varies between 5-10 minutes on an IBM 320 RISC/6000 workstation. For the Re=800 case, an additional multigrid level is added to ensure grid independence and the CPU required is increased to approximately 30 minutes on the same workstation. All solutions are initiated with uniform flow approximations and Reynolds number continuation is not required, even for the relatively complex Re=800 case. Grid convergence has been established efficiently through an adaptive multigrid procedure. The outflow boundary condition has been shown to be non-reflective. In addition, it has been shown that the procedure is not very sensitive to the location of the outflow, i.e. far downstream or somewhat closer to the inflow. The flux-split discretization allows for direct computation of the normal velocity and therefore mass conservation at grid interfaces and subdomain boundaries is achieved in a simple fashion.

Acknowledgement

This research was supported in part by the NASA Lewis Research Center (J. Adamczyk, Technical Monitor), Grant No. NAG-397 and by the AFOSR (L. Sakell, Technical Monitor), Grant No. 90-0096. The Cray Y-MP at the Ohio Supercomputer was used for these computations.

References

1. Rubin, S.G. and Reddy, D.R., "Analysis of Global Pressure Relaxation for Flows With Strong

Interaction and Separation", Computers and Fluids, 11, pp. 281-306, 1983.
2. Rubin, S.G., "Incompressible Navier-Stokes and Parabolized Navier-Stokes Formulations and Computational Techniques", Computational Methods in Viscous Flows, Vol. 3, W. Habashi, Ed., Pineridge Press, pp. 53-99, 1984.
3. Rubin, S.G., "RNS/Euler Pressure Relaxation and Flux Vector Splitting, Computers and Fluids, 16, pp. 485-490, 1988.
4. Fuchs, L., "A Local Mid-Refinement Technique for Incompressible Flows", Computer and Fluids, 14, pp. 69-81, 1986.
5. Thompson, M.C. and Ferziger, J.H., "An Adaptive Multigrid Technique for the Incompressible Navier-Stokes Equations", J. of Comp. Physics, 82, pp. 94-121, 1989.
6. Srinivasan, K. and Rubin, S.G., "Adaptive Multigrid Domain Decomposition Solutions of the Reduced Navier-Stokes Equations", Proceedings of Fifth SIAM Conference on Domain Decomposition Methods for Partial Differential Equations, Norfolk, VA., May 1991.
7. Srinivasan, K. and Rubin, S.G., "Flow Over a Backward Facing Step Using the Reduced Navier-Stokes Equations", Proceedings of the Minisymposium on Outflow Boundary Conditions, Stanford University, July 1991.
8. Srinivasan, K. and Rubin, S.G., "Adaptive Multigrid Domain Decomposition Solutions for Incompressible Viscous Flows", submitted to Int'l J. Num. Methods in Fluids.
9. Himansu, A. and Rubin, S.G., "Multigrid Acceleration of a Relaxation Procedure for the Reduced Navier-Stokes Equations", AIAA J., 26, pp. 1044-1051, 1988.
10. Rubin, S.G. and Himansu, A., "Convergence Properties of High Reynolds Number Separated Flow Calculations", Int'l J. Num. Methods in Fluids, 9, pp. 1395-1411, 1989.
11. Rosenfeld, M. and Israeli, M., "Numerical Solution of Incompressible Flows by a Marching Multigrid Nonlinear Method", AIAA J., 25, pp. 641-47, 1987.
12. Brandt, A., "Multi-level Adaptive Solutions to Boundary Value Problems", Mathematics of Computation, 31, pp. 333-390, 1977.
13. Sotiropoulos, F., "A Primitive Variable Method for the Solution of External and Internal Incompressible Flow Fields", Ph.D Dissertation, University of Cincinnati, 1991.
14. Gartling, D.K., "A Test Problem for Outflow Boundary Condition - Flow Over Backward Facing Step", Int'l Journal of Num. Meth. in Fluids, 11, pp. 953-967, 1990.
15. Caruso, S., "Adaptive Grid Techniques for Fluid Flow Problems", Ph.D Thesis, Thermosciences Division, Department of Mechanical Engineering, Stanford University, California, 1985.
16. Thangam, S. and Spezial, C.G., "Turbulent Separated Flow Past a Backward Facing Step: A Critical Evaluation of Two-Equation Turbulence Models, ICASE Report No. 91-23, February 1991.
17. Thangam, S., "Analysis of Two-Equation Turbulence Models for Recirculating Flows", ICASE Report No. 91-61, July 1991.
18. Eaton, J. and Johnston, J.P., "Turbulent Flow Reattachment: An Experimental Study of the Flow and Structure Behind a Backward Facing Step", Technical Report MD-39, Stanford University, California, 1980.

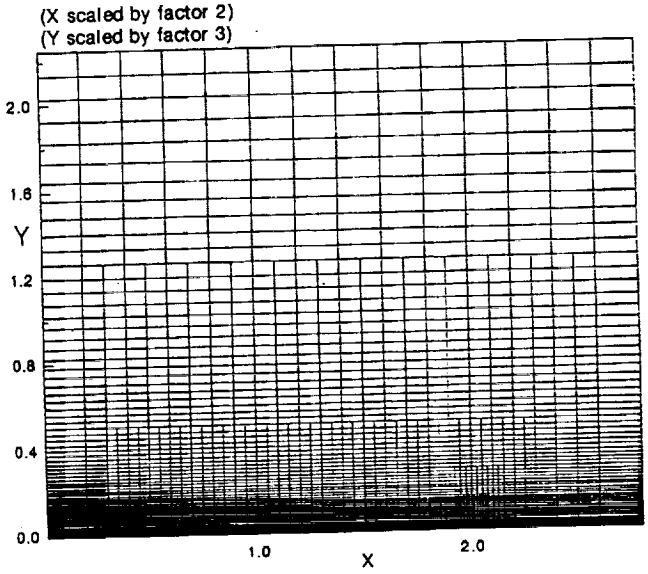

Figure 1. Multigrid levels (one-dimensional adaptivity); trailing edge flow ($Re=10^5$)

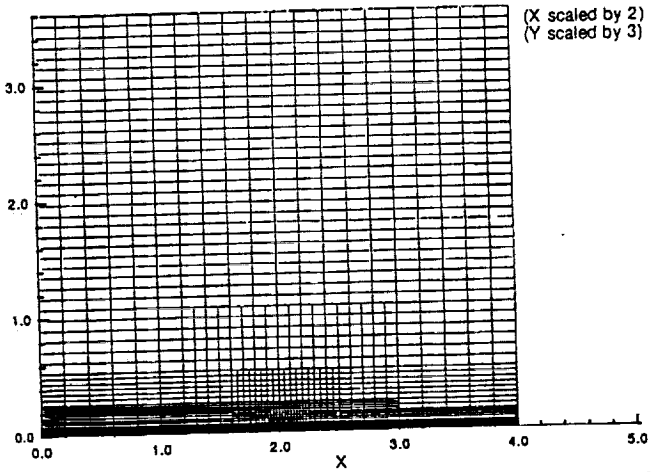

Figure 2. Multigrid levels (two-dimensional adaptivity); trailing edge flow ($Re=10^5$)

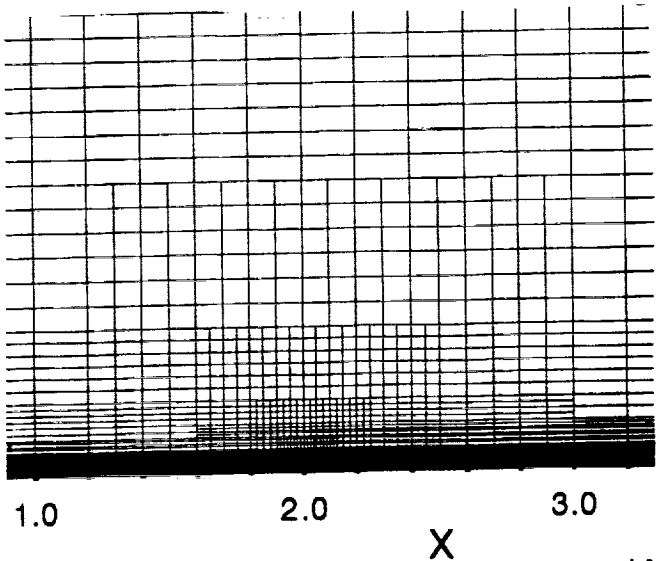

Figure 2a. Enlargement of the fine grid region in Figure 2.

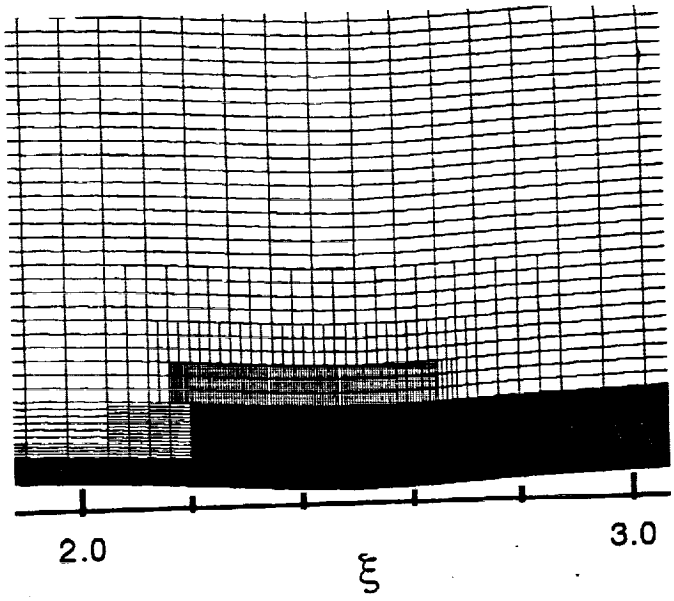

Figure 4a. Enlargement of the fine grid region in Figure 4.

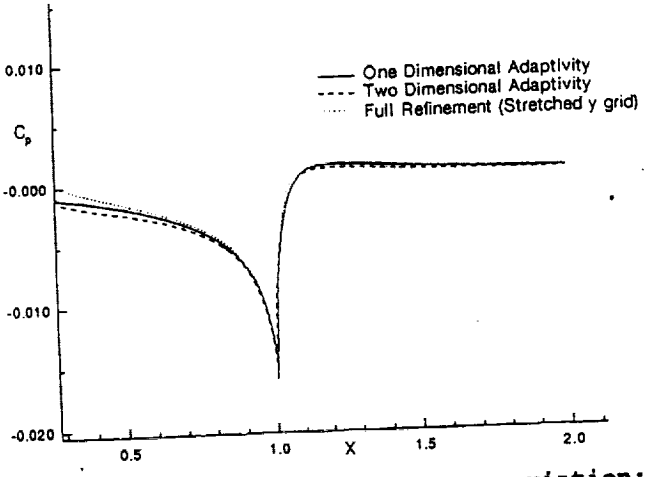

Figure 3. Comparison of c_p variation; trailing edge flow ($Re=10^5$)

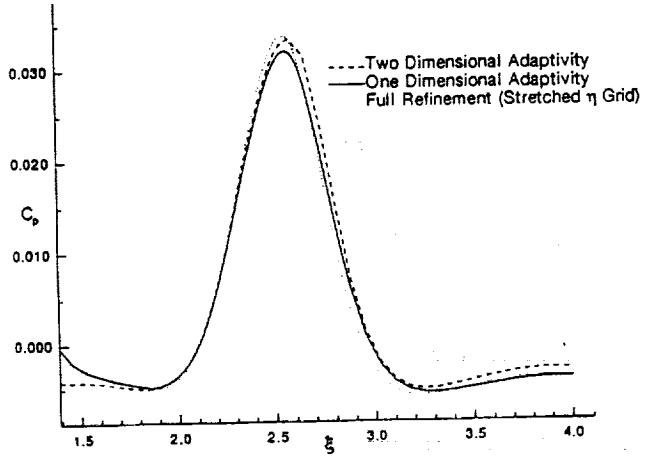

Figure 5. Comparison of c_p variation; unseparated flow past trough (D=0.015, Re=80000)

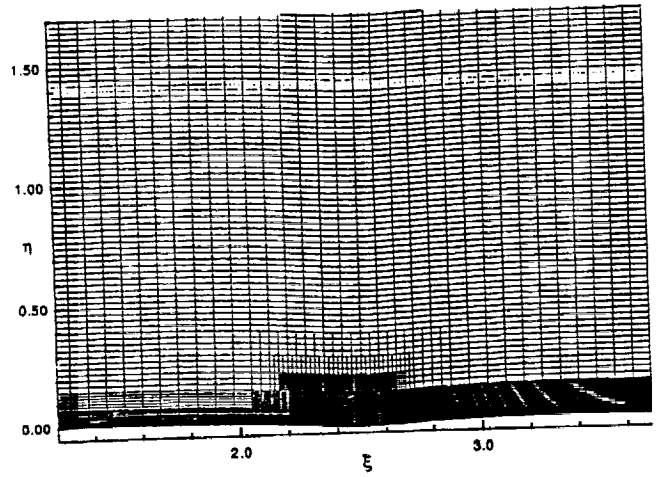

Figure 4. Multigrid levels (two-dimensional adaptivity) separated flow past trough (D=0.03, Re=80000)

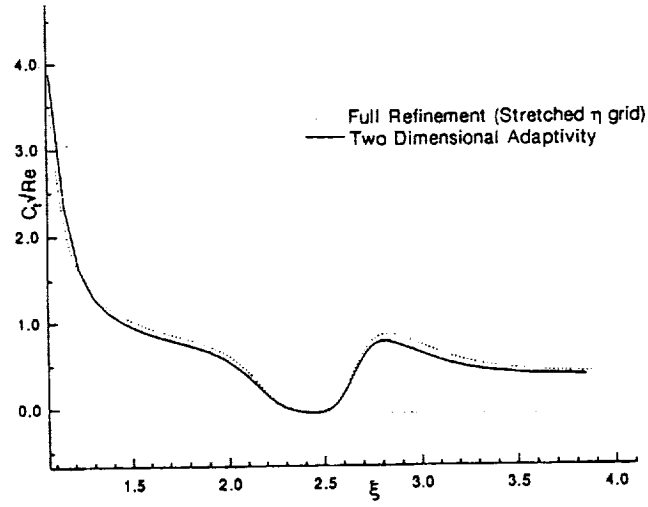

Figure 6. Comparison of skin friction parameter; separated flow past trough (D=0.03, Re=80000)

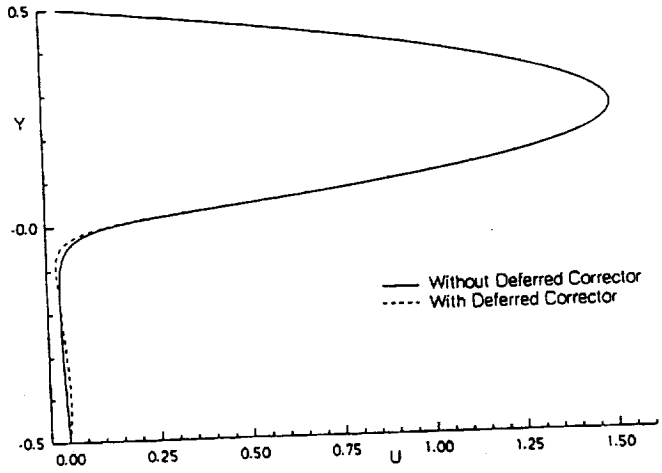

Figure 7a. Comparison of streamwise velocity profile at x=0.0625; Backward facing step (Re=400)

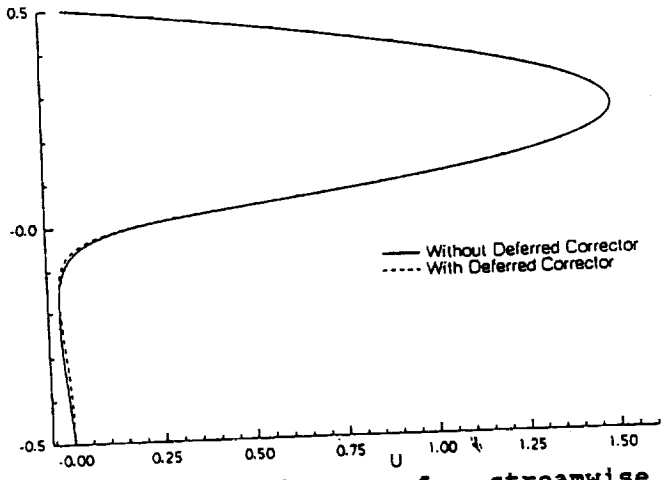

Figure 7b. Comparison of streamwise velocity profile at x=0.125; Backward facing step (Re=400)

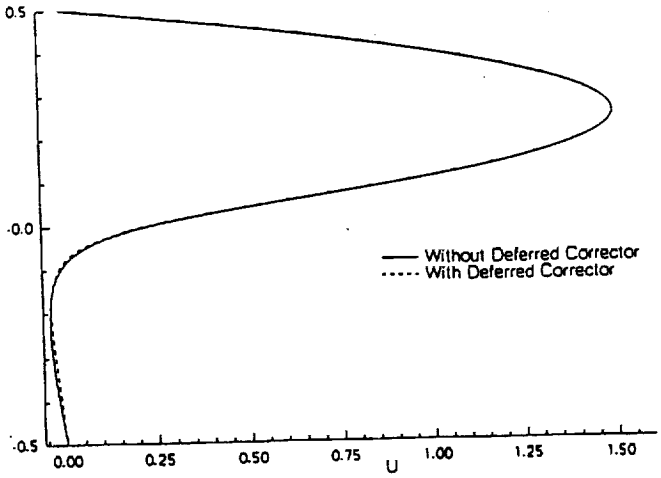

Figure 7c. Comparison of streamwise velocity profile at x=0.1875; Backward facing step (Re=400)

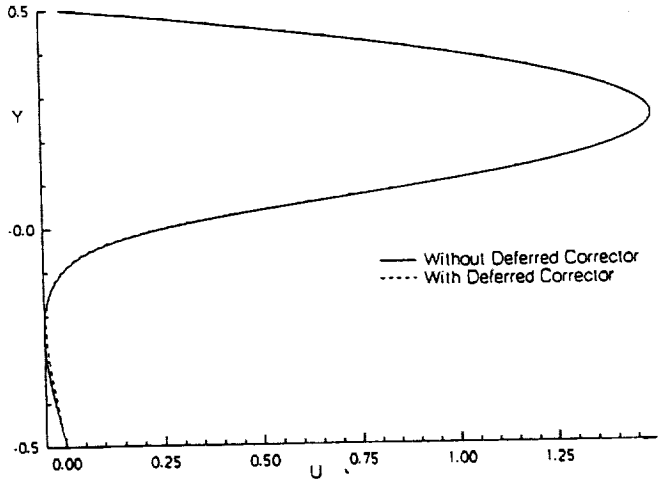

Figure 7d. Comparison of streamwise velocity profile at x=0.25; Backward facing step (Re=400)

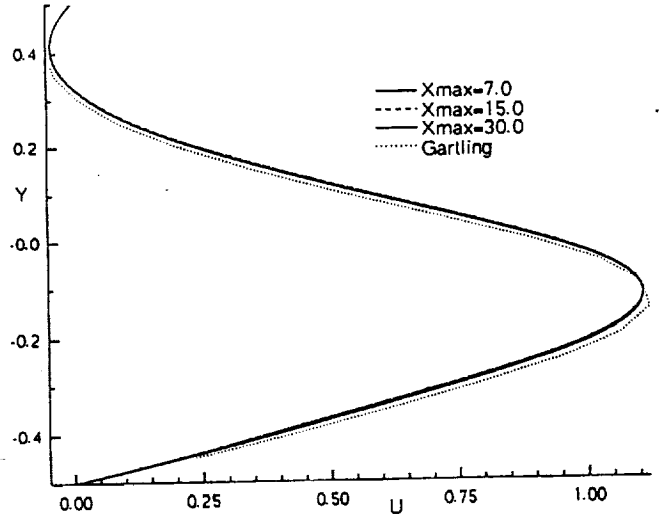

Figure 8. Comparison of streamwise velocity profile at x=7; Effect of location of outflow boundary; Backward facing step (Re=800)

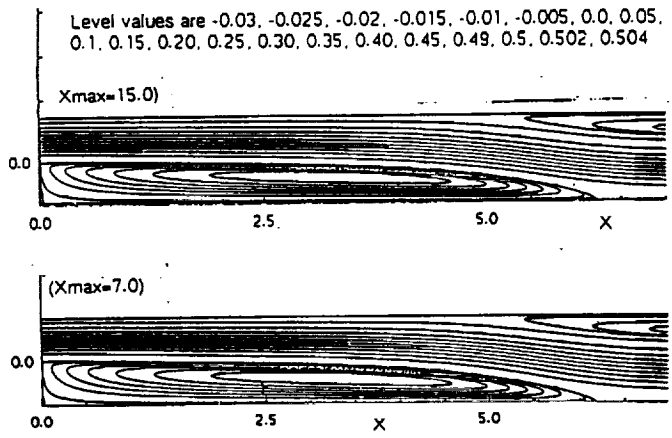

Figure 9. Comparison of streamfunction contours; effect of location of outflow boundary; Backward facing step (Re=800)

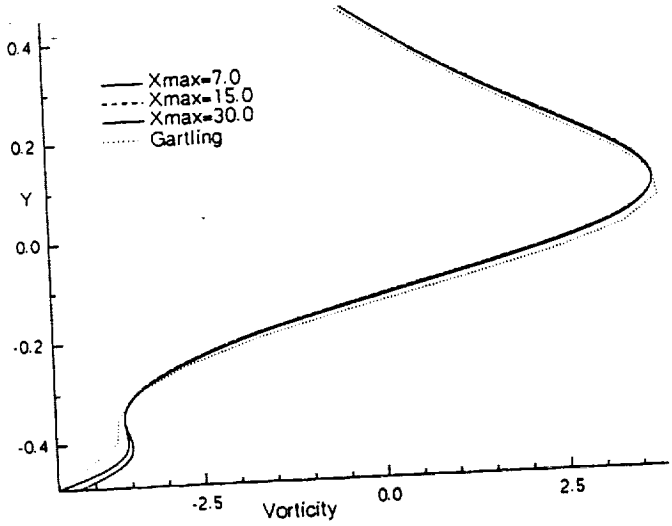

Figure 10. Comparison of vorticity profiles at x=7.0; Backward facing step (Re=800)

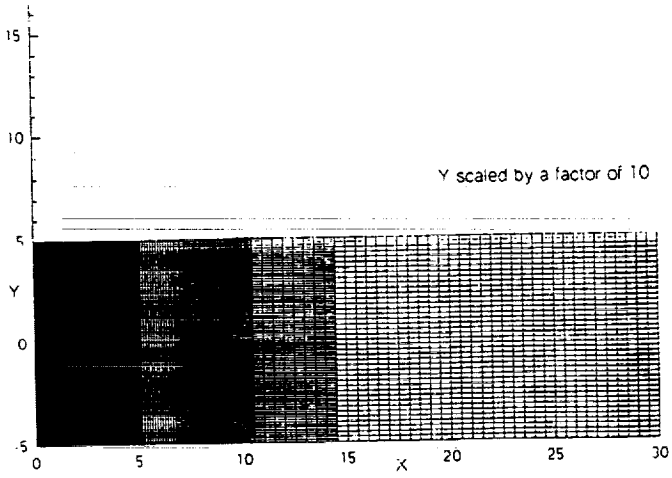

Figure 12. Multigrid levels; Backward facing step (Re=267)

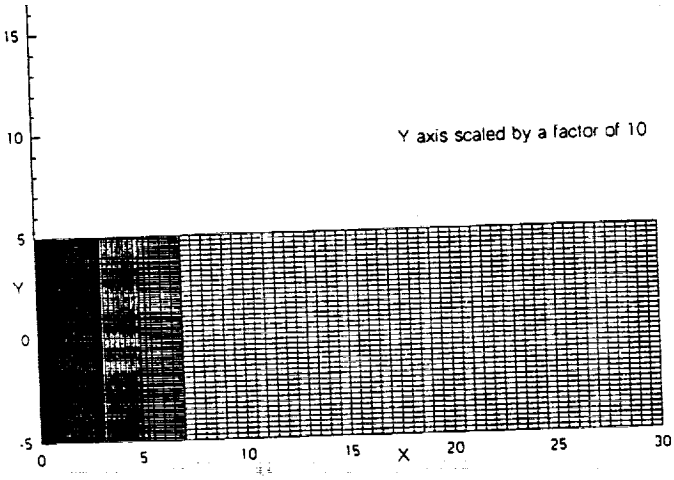

Figure 11. Multigrid levels; Backward facing step (Re=100)

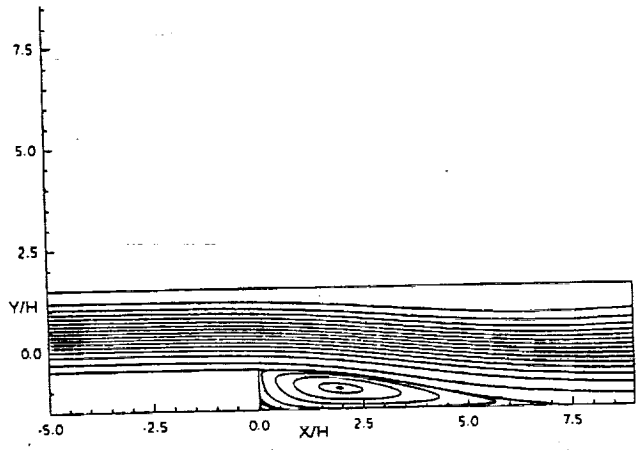

Figure 13. Streamfunction contours; Backward facing step (Re=132000)